Mechanisms of Monovalent Cation Action in Enzyme Catalysis: The Tryptophan Synthase α-, β-, and αβ-Reactions†

Eilika Woehl‡ and Michael F. Dunn*

Department of Biochemistry, University of California at Riverside, Riverside, California 92521

Received December 11, 1998; Revised Manuscript Received March 29, 1999

ABSTRACT: The α-subunit of the tryptophan synthase bienzyme complex catalyzes the formation of indole from the cleavage of 3-indolyl-D-glyceraldehyde 3′-phosphate, while the β-subunit utilizes L-serine and the indole produced at the α-site to form tryptophan. The replacement reaction catalyzed by the β-subunit requires pyridoxal 5′-phosphate (PLP) as a cofactor. The β-reaction occurs in two stages: in stage I, the first substrate, L-Ser, reacts with the enzyme-bound PLP cofactor to form an equilibrating mixture of the L-Ser Schiff base, E(Aex_1), and the α-aminoacrylate Schiff base intermediate, E(A-A); in stage II, this intermediate reacts with the second substrate, indole, to form tryptophan. Monovalent cations (MVCs) are effectors of these processes [Woehl, E., and Dunn, M. F. (1995) *Biochemistry 34*, 9466−9476]. Herein, detailed kinetic dissections of stage II are described in the absence and in the presence of MVCs. The analyses presented complement the results of the preceding paper [Woehl, E., and Dunn, M. F. (1999) *Biochemistry 38*, XXXX−XXXX], which examines stage I, and confirm that the chemical and conformational processes in stage I establish the presence of two slowly interconverting conformations of E(A-A) that exhibit different reactivities in stage II. The pattern of kinetic isotope effects on the overall activity of the β-reaction shows an MVC-mediated change in rate-limiting steps. In the absence of MVCs, the reaction of E(A-A) with indole becomes the rate-limiting step. In the presence of Na^+ or K^+, the conversion of E(Aex_1) to E(A-A) is rate limiting, whereas some third process not subject to an isotope effect becomes rate determining for the NH_4^+-activated enzyme. The combined results from the preceding paper and from this study define the MVC effects, both for the reaction catalyzed by the β-subunit and for the allosteric communication between the α- and β-sites. Partial reaction-coordinate free energy diagrams and simulation studies of MVC effects on the proposed mechanism of the β-reaction are presented.

The tryptophan synthase bienzyme complex ($\alpha_2\beta_2$) from *Salmonella typhimurium* carries out an unusual combination of chemical reactions (Scheme 1) and physical transformations involving two different catalytic sites located on separate subunits (Figure 1); see also the preceding paper (*1*). This bienzyme complex catalyzes the last two steps in the biosynthesis of L-tryptophan (L-Trp[1]) from 3-indolyl-D-glycerol 3′-phosphate (IGP) and L-serine (L-Ser) (Scheme 1) (*2*−*5*). It is now well established that the indole produced at the α-site is transferred to the β-site via a 25 Å long interconnecting tunnel (Figure 1) where reaction with L-Ser gives L-Trp (*6*−*15*). The relationship between the architecture of the bienzyme complex and the dynamic events involving the chemistry and the conformational transitions in the protein is now fairly well understood (*6*, *16*−*18*). To achieve efficient utilization of indole, the catalytic cycles of the α- and β-reactions (Figure 1) are phased to each other via an allosteric signaling mechanism (*7*, *10*, *13*, *15*, *18*) in which the α-site is switched on by the conversion of the L-Ser external aldimine, E(Aex_1), to the α-aminoacrylate Schiff base intermediate, E(A-A) (*10*) (viz., Scheme 1B).

Following the cleavage of IGP at the α-site, diffusion of indole along the tunnel into the β-site, reaction with E(A-A) to form the L-Trp quinonoid, E(Q_3), and conversion of E(Q_3) to the L-Trp external aldimine, E(Aex_2) (viz., Scheme 1B), the α-site is switched off again (*13*). The switching on and off is accompanied by conformational transitions between open states with low α-site activity and closed states with high α-site activity (Scheme 1B and Figure 1) (*11*, *12*, *17*, *18*). This cycle of switching between inactive (open) and active (closed) states forces the catalytic cycles of the two enzymes to occur in phase and prevents the escape of indole (*18*).

† Supported by NIH Grant GM55749 and NSF Grant MCB-9218902 (E.W.).

* Corresponding author. Phone: 909-787-4235. Fax: 909-787-4434. E-mail: michael.dunn@ucr.edu.

‡ Present address: Howard Hughes Medical Institute, School of Medicine, Yale University, New Haven, CT 06510.

[1] Abbreviations: $\alpha_2\beta_2$, the tryptophan synthase bienzyme complex; β_2, the β-subunit dimer species; IGP, 3-indolyl-D-glycerol 3′-phosphate; IPP, 3-indolyl-propanol 3′-phosphate; 5-fluoro-IGP, the 5-fluoro derivative of IGP; G3P, D-glyceraldehyde 3-phosphate; GP, α-glycerophosphate; L-Ser (or S) and D,L-Ser, L-serine and D,L-serine, respectively; In, indole; L-Trp, L-tryptophan; PLP, pyridoxal 5′-phosphate; KIE, kinetic isotope effect; SWSF single-wavelength stopped-flow; RSSF, rapid-scanning stopped-flow. The various covalent forms of PLP-bound serine at the β-site (see Scheme 1) are designated as follows: E(Ain) or E, the internal aldimine (Schiff base); E(GD_1), the first *gem*-diamine species; E(Aex_1), the L-Ser external aldimine (Schiff base); E(Q_1), the L-Ser quinonoid; E(A-A), the α-aminoacrylate Schiff base; E(Q_2), the quinonoid formed initially in the Michael addition of indole with E(A-A); E(Q_3), the quinonoid formed by abstraction of a proton from E(Q_2); E(Aex_2), the L-Trp external aldimine (Schiff base); E(GD_2), the L-Trp *gem*-diamine.

10.1021/bi982919p CCC: $18.00
Published on Web 05/11/1999

Scheme 1: Organic Chemistry of the α- and β-Reactions[a]

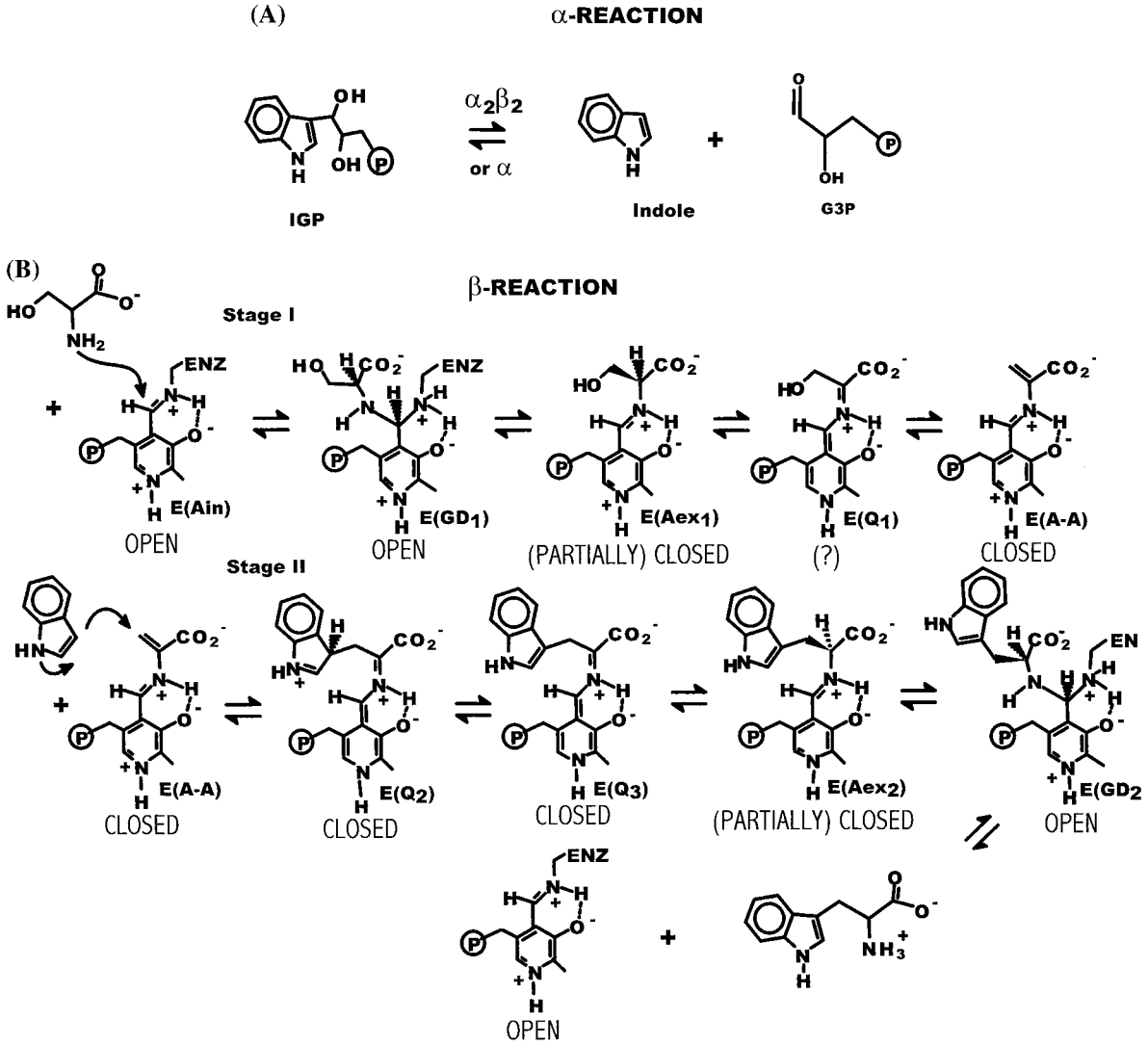

[a] The α-reaction is shown as a simple, reverse aldol-like cleavage reaction. The β-reaction occurs in two stages. In stage I, L-Ser reacts with enzyme-bound PLP to give the Schiff base of α-aminoacrylate, E(A-A). In stage II, E(A-A) reacts with indole to give L-Trp. OPEN, CLOSED, and (PARTIALLY) CLOSED designate protein conformations.

The allosteric signaling triggered by the above-described covalent changes at the β-site occurs via a network of protein and cofactor structural elements linking the α- and β-sites. This network includes a monovalent cation (MVC) cofactor site located in the β-subunit about 8 Å distant from the β-catalytic site (*1*, *16*−*20*). The protein linkages between the MVC site and the α- and β-catalytic sites include two salt bridges involving two alternative orientations of a lysine residue in the β-subunit (βK167), loop structures which fold down over the α-site to make a closed conformation (*11*, *12*), and a domain movement in the β-subunit which closes the entrance to the β-site (*1*, *11*, *12*, *17*) (Figure 2).

The reaction of L-Ser with indole at the β-site occurs in two stages (Scheme 1B). In stage I, L-Ser reacts with enzyme-bound PLP to form E(A-A),[1] a quasi-stable species poised to react with indole. In stage II, the electron-rich C3 of indole makes a nucleophilic attack on the electrophilic Cβ of the α-aminoacrylate species to give a quinonoidal species, $E(Q_2)$, that is rapidly deprotonated to $E(Q_3)$, which then is converted to L-Trp via the $E(Aex_2)$ and $E(GD_2)$ species (Scheme 1). In this work, we examine the roles played by the binding of MVCs in modulating the chemical and conformational processes involved in stage II of the β-reaction and in the αβ-reaction.

MATERIALS AND METHODS

The materials and methods used in this work were the same as those described in the preceding paper (*1*).

RESULTS

Single-Wavelength Absorbance Stopped-Flow Kinetic Analysis of the Second Stage of the β-Reaction. The second stage of the β-reaction, the reaction of E(A-A) with indole to form L-Trp, was investigated for indole concentrations ranging from 0.2 to 2.0 mM. The formation and decay of the $E(Q_3)$ species were followed at 476 nm. Under these conditions, the process is biphasic (*21*, *22*) with a fast, increasing phase of $E(Q_3)$ formation followed by a slower, decreasing phase (see Figure 3A). Figure 3B shows the dependence of the relaxation rate constant determined for the fast process on the indole concentration in the absence and in the presence of NaCl.

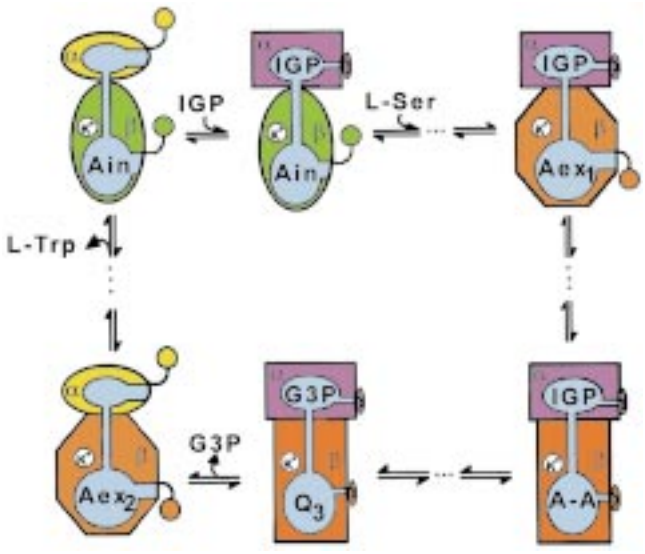

FIGURE 1: Conformation states of the catalytic cycle. Cartoon depicting the linkage of binding interactions and covalent changes at the α- and β-sites to the cycle of conformation changes in αβ-subunit pairs during the synthesis of L-Trp from IGP and L-Ser. The MVC site is shown occupied by K^+. The bound/covalent states of the α- and β-sites are indicated by the acronyms for the various covalent states of the reacting substrates.[1] Ellipses designate open conformations, squares designate closed conformations, and octagons designate partially closed conformations. Activation of the α-site occurs when $E(Aex_1)$ is converted to E(A-A); deactivation occurs when $E(Q_3)$ is converted to $E(Aex_2)$. Redrawn from Pan et al. (*18*) with permission.

To determine the kinetic parameters for this reaction, the simplified mechanism shown in eq 1 was assumed. After

$$\text{indole} + \text{E(A-A)} \underset{k_{-1}}{\overset{k_1}{\rightleftharpoons}} \text{E(A-A)(indole)} \underset{k_{-2}}{\overset{k_2}{\rightleftharpoons}} \text{E}(Q_3) \underset{k_{-3}}{\overset{k_3}{\rightleftharpoons}} \text{E}(Aex_2) \quad (1)$$

formation of the Michaelis complex, E(A-A)(indole), the second stage of the β-reaction proceeds through two quinonoidal intermediates, $E(Q_2)$ and $E(Q_3)$ (Scheme 1). However, $E(Q_2)$ converts to $E(Q_3)$ more rapidly than it is formed and, consequently, cannot be detected. Therefore, $E(Q_2)$ is neglected in the above mechanism. From previous work (*20*−*22*) it is known that equilibration of the first step is much faster than that of the second and third steps; thus it can be assumed that

$$k_1[\text{indole}] + k_{-1} \gg k_2, k_{-2}, k_3, k_{-3} \quad (2)$$

By analogy to the relaxation expressions formulated for stage I of the L-Ser reaction (*1*), the dependence of the relaxation rates on the concentration of indole is then described by eqs 3−6.

$$\frac{1}{\tau_2\tau_3} = k_2(k_3 + k_{-3})\frac{K_1[\text{indole}]}{1 + K_1[\text{indole}]} + k_{-2}k_{-3} \quad (3)$$

$$\frac{1}{\tau_2\tau_3 - (k_{-2}k_{-3})} = \frac{1}{k_2K_1(k_3 + k_{-3})}\frac{1}{[\text{indole}]} + \frac{1}{k_2(k_3 + k_{-3})} \quad (4)$$

$$\frac{1}{\tau_2} + \frac{1}{\tau_3} = k_2\frac{K_1[\text{indole}]}{1 + K_1[\text{indole}]} + k_{-2} + k_3 + k_{-3} \quad (5)$$

$$\frac{1}{(\tau_2^{-1} + \tau_3^{-1})(k_{-2} + k_3 + k_{-3})} = \frac{1}{k_2K_1}\frac{1}{[\text{indole}]} + \frac{1}{k_2} \quad (6)$$

Table 1 summarizes the kinetic and equilibrium parameters for stage II ($K_1 = k_{-1}/k_1$, k_2, k_{-2}, k_3, and k_{-3}) determined via the above treatment for reaction both in the absence and in the presence of NaCl. These results show that the rate parameters for the forward reaction do not change significantly upon addition of NaCl, whereas k_{-2} is strongly decreased; consequently, the amplitude of the observed signal increases because the reverse rate constant for the second step is reduced by more than 10-fold in the presence of the metal ion.

Dependence of Stage II on NaCl. The reaction of E(A-A) with indole was followed using the change in absorbance at

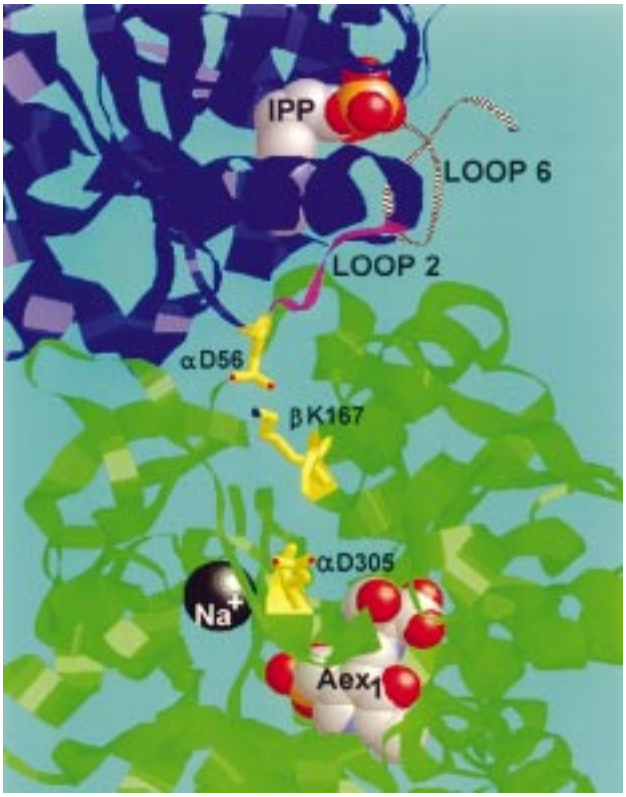

FIGURE 2: Ribbon diagram of an αβ-dimeric unit of the tryptophan synthase mutant βK87T with the IGP analogue 3-indolylpropanol-3′-phosphate bound to the α-site and the L-Ser external aldimine of PLP bound to the β-site. Coordinates were taken from 2TRS.PDB (*17*), and the drawing was constructed using RasMol 2. The structure is viewed perpendicular to the interconnecting tunnel, and both the α- and β-sites are in closed conformations with access to solvent blocked. Cofactors and ligands are shown as space-filling models. Residues believed to be important for the communication of allosteric signals between the α- and β-sites are shown as yellow sticks (i.e., αD56 with side chain O red, βK167 with side chain N blue, and αD305 with side chain O red). Loops 2 and 6, which fold down over the α-site to make a closed structure, are shown in magenta and red. Due to disorder in the structure, loop 6 is truncated at residue 187 in the PDB data file. Color scheme: α-subunit, blue; β-subunit, green; α-loop 2, magenta; α-loop 6, black stripes; stick models of individual amino acid residues, yellow; Na^+, black; ligand C, silver; ligand O, red; ligand N, blue; ligand P, orange.

Table 1: Influence of NaCl on the Kinetic Parameters for Stage II of the β-Reaction[a,b]

reaction conditions	K_1 (mM^{-1})	k_2 (s^{-1})	k_{-2} (s^{-1})	k_3 (s^{-1})
E(A-A) + indole	1.5	270	20	50
E(A-A) + indole + NaCl	3.8	270	1	50

[a] Kinetic parameters were obtained from the fitting of the data in Figure 3 to eqs 3−6 (see text). [b] Error limits for rate and equilibrium parameters are estimated to be as follows: K_1, ±10%; k_2, ±5%; k_{-2}, ±15%; k_3, ±10.

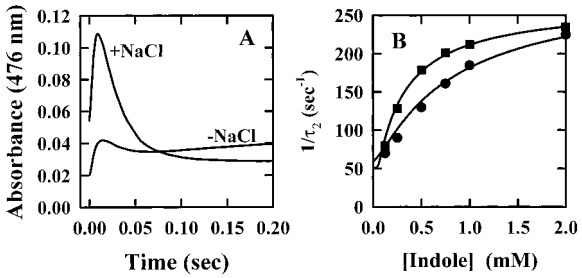

FIGURE 3: Dependence of the reaction of E(A-A) with indole on varying concentrations of indole in the presence and absence of Na^+. Panel A shows the time courses for the formation and decay of the quinonoidal species in the absence and in the presence of 100 mM NaCl for one of the titration points (1 mM indole). In panel B, the relaxation rate constant ($1/\tau_2$) for the fast phase of quinonoid formation (measured at λ_{max} = 476 nm) is plotted as a function of [indole]. Concentrations: $[\alpha_2\beta_2]$ = 15 μM, [L-Ser] = 40 mM, and [NaCl] = 100 mM where present. Symbols: circles, absence of NaCl; squares, presence of 100 mM NaCl.

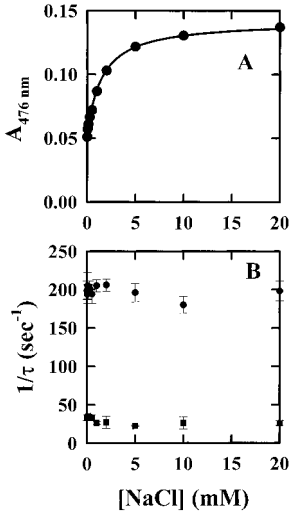

FIGURE 4: Dependence of quinonoid yield and relaxation rate in the reaction of indole with E(A-A) as a function of [NaCl] measured in SWSF experiments using the transient quinonoidal peak with λ_{max} = 476 nm as the signal. Panel A shows the absorbance maximum of the transient peak as a function of NaCl. Panel B shows the concentration dependence of the relaxation rate constants both on the formation and on the decay of the quinonoidal species. Concentrations: $[\alpha_2\beta_2]$ = 10 μM, [L-Ser] = 40 mM, and [indole] = 5 mM.

476 nm due to $E(Q_3)$. Figure 4 shows the effects of the NaCl concentration both on the maximum amplitude of the quinonoid peak (A) and on the relaxation rate constants for the formation ($1/\tau_1$, circles) and decay ($1/\tau_2$, squares) of this band (B). The relaxation rate constants for the formation and the decay of the quinonoid were found to be essentially independent of the NaCl concentration. The amplitudes of these relaxations (Figure 4A), however, increase and then

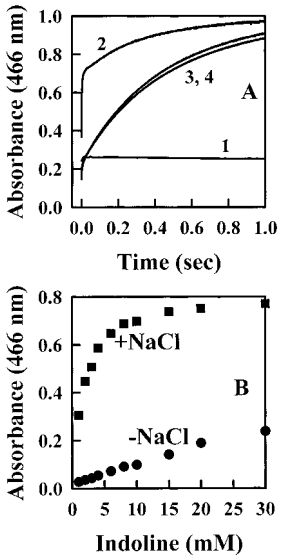

FIGURE 5: Reaction of E(A-A) with the indole analogue, indoline. (A) SWSF time traces are shown for the reaction in the absence and in the presence of 100 mM NaCl (traces 1 and 2, respectively). The reaction of metal-free E(A-A) with a mixture of indoline and NaCl is shown for the condition where NaCl is present in the substrate syringe only (trace 3) and for the condition where indoline and E(A-A) are premixed in one syringe and then mixed with NaCl from the other syringe (trace 4). Concentrations: $[\alpha_2\beta_2]$ = 19 μM, [L-Ser] = 40 mM, [indoline] = 2 mM, and [NaCl] = 100 mM where present. (B) Dependence of the amplitude of the quasi-stable $E(Q)_{indoline}$ peak on the indoline concentration in the absence of NaCl (circles), and in the presence of NaCl (squares). Concentrations: $[\alpha_2\beta_2]$ = 7.6 μM, [L-Ser] = 40 mM, and [NaCl] = 100 mM where present.

become concentration independent with increasing NaCl concentration.

Formation of a Quasi-Stable Quinonoidal Species with the Indole Analogue Indoline in the Presence and Absence of Metal Ion. To further characterize the events occurring during stage II, the reaction of the indole analogue, indoline, with E(A-A) was examined in detail. When E(A-A) (formed in a preequilibrated mixture of $\alpha_2\beta_2$ and L-Ser) is reacted with indoline, the formation of the indoline quinonoid, $E(Q)_{indoline}$ (λ_{max} = 466 nm), is very rapid, whereas turnover of this quinonoid occurs very slowly to give the tryptophan analogue dihydroiso-L-tryptophan (*10*−*12*, *23*), making $E(Q)_{indoline}$ a quasi-stable species (*23*). To investigate MVC effects on this reaction, the appearance of $E(Q)_{indoline}$ resulting from reaction of $\alpha_2\beta_2$ with premixed L-Ser and indoline was measured both in the absence and in the presence of NaCl under a variety of premixing conditions.

Figure 5A shows the time courses for $E(Q)_{indoline}$ formation in the absence of NaCl (trace 1), in the presence of NaCl (trace 2), with NaCl present in the substrate syringe only (trace 3), and with $E(Q)_{indoline}$ preformed from premixed E(A-A) and indoline and then reacted with NaCl (trace 4). In the absence of the metal ion, $E(Q)_{indoline}$ accumulates to only about 8% of the β-sites in a monophasic process with a relaxation rate constant of about 500 s^{-1} (trace 1). In the presence of NaCl (trace 2), $E(Q)_{Indoline}$ appears in two phases, one fast phase with a relaxation rate constant of 450 s^{-1} and another, slower phase with a relaxation rate constant of 2.7 s^{-1}. At the same concentration of indoline (2 mM), and when the reaction mixture is preequilibrated with indoline, the final amount of accumulated $E(Q)_{indoline}$ equals 55% of the β-sites,

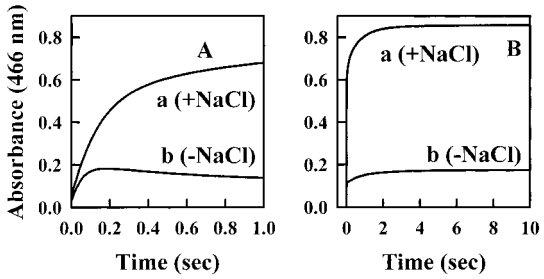

FIGURE 6: (Panel A) Reaction of $\alpha_2\beta_2$ with a mixture of L-Ser and indoline in the absence (b) and in the presence (a) of NaCl. (Panel B) Reaction of a preequilibrated mixture of $\alpha_2\beta_2$ and L-Ser with indoline in the absence (b) and in the presence (a) of NaCl. Concentrations: $[\alpha_2\beta_2] = 10\ \mu M$, [L-Ser] = 40 mM, [indoline] = 10 mM, and [NaCl] = 100 mM where present.

out of which 36% form in the fast phase and 19% form in the slow phase. The percentages refer to total β-sites and were estimated from the amplitudes assuming that the absorbance at saturation from the titration curve in the presence of NaCl (Figure 5B) corresponds to the condition where 100% of the β-sites are in the form of $E(Q)_{indoline}$. In the case where NaCl is present only in the substrate syringe (trace 3), about 8% forms in the fast phase and 46% forms more slowly with relaxation rate constants of ~1.5 to ~3 s^{-1}. When $E(Q)_{indoline}$ is preformed prior to reaction with NaCl (trace 4), only a slow phase of formation can be observed in which ~46% of the β-sites react to form $E(Q)_{indoline}$, again at rates of ~3 to ~1.5 s^{-1}.

Figure 5B shows the dependence of the absorbance at 466 nm on the indoline concentration, both in the absence and in the presence of NaCl, measured about 10 s after reaction with $\alpha_2\beta_2$. The titration curve measured in the presence of NaCl shows much tighter apparent binding than does the titration curve measured in the absence of NaCl.

To investigate the kinetic behavior at higher concentrations of indoline, either $\alpha_2\beta_2$ was reacted with a mixture of L-Ser and 10 mM indoline (Figure 6A) or preformed E(A-A) was reacted with 10 mM indoline (Figure 6B), with both experiments carried out in the presence and in the absence of NaCl. In the presence of NaCl after rapid reaction of $\alpha_2\beta_2$ with a mixture of L-Ser and indoline, the appearance of $E(Q)_{indoline}$ is biphasic (panel A, trace a) with relaxation rate constants of 7 and 1 s^{-1}, respectively. The total accumulation of $E(Q)_{indoline}$ equals 80% of the β-sites with ~50% forming in the faster phase. In the absence of MVCs (panel A, trace b), $E(Q)_{indoline}$ accumulates to a final amount of ~16% of the β-sites, all of which is formed in one phase with a relaxation rate constant of 19 s^{-1}. A decreasing phase with a small amplitude can also be detected. Formation of $E(Q)_{indoline}$ from a preequilibrated mixture of enzyme and L-Ser in the presence of NaCl (panel B, trace a) gave a triphasic trace with 54% formed in a fast relaxation (~925 s^{-1}, with an amplitude that is ~50% of the total change), less than 8% formed in an intermediate phase (~10 s^{-1}), and the remainder formed in a slow process (~1.3 s^{-1}). In the absence of MVCs (panel B, trace b), up to 6% of the enzyme sites react in a fast process of ~700−800 s^{-1} (the small amplitude makes the rate estimation difficult), and approximately 11% react in a much slower process (~2 s^{-1}).

Kinetic Isotope Effects on Individual Steps of the β-Reaction. Single-wavelength stopped-flow time courses were measured at 350 nm for the second stage of the β-reaction (data not shown). The band at 350 nm is a component of the E(A-A) spectrum and, therefore, serves as a signal for E(A-A) formation and decay (*14*). In the reaction of the E(A-A) species with indole to form $E(Q_3)$, the Cβ of L-Ser changes hybridization state from sp^2 to sp^3, a transformation that exhibits an inverse secondary KIE (*13*). When the disappearance of the E(A-A) species is followed at 350 nm, the reaction in the absence of MVCs is biphasic with a fast phase of about 140 s^{-1} and a second phase about 100-fold slower (Table 2). In the presence of NaCl, there is an additional decreasing phase with a rate of ~30 s^{-1}. In the presence of NH_4Cl, there also is an additional phase that is intermediate in rate, but which arises from an increase in absorbance. In the absence of MVCs, the amplitude of the fast phase is much smaller than in the presence of either NaCl or NH_4Cl. In all cases, only the fast phase shows the inverse secondary isotope effect; the slower phases are not subject to an isotope effect. Table 2 shows the curve-fitting results for the corresponding time courses.

Primary and Secondary Isotope Effects on Enzyme Activity. Steady-state activity measurements for the β- and $\alpha\beta$-reactions were performed to investigate the rate-limiting character of individual steps both in the absence and in the presence of MVCs (Table 3). The β-reaction was tested using isotopically normal D,L-Ser and [β-^{2}H]-D,L-Ser. When D,L-

Table 2: Comparison of MVC Effects on Relaxation Rate Constants and Secondary KIEs Measured for Stage II of the β-reaction[a,b]

Ser isotope and MVC effector	$1/\tau_1$	KIE (H/D)	$1/\tau_2$	KIE (H/D)	$1/\tau_3$	KIE (H/D)
D,L-Ser; no MVCs	138				1.6	
[β-^{2}H]-D,L-Ser; no MVCs	169	0.82			1.7	1
D,L-Ser; NaCl	171		29		2.8	
[β-^{2}H]-D,L-Ser; NaCl	226	0.76	25	1.1	2.5	1.1
D,L-Ser; NH_4Cl	129		55		2.7	
[β-^{2}H]-D,L-Ser; NH_4Cl	195	0.66	36	1.5	2.7	1

[a] Relaxation rate constants were measured for the disappearance of E(A-A) measured at 350 nm. E(A-A) was preformed in one syringe of the stopped-flow apparatus (via reaction of $\alpha_2\beta_2$ with serine) with indole in the other syringe both in the absence of MVCs and in the presence of 100 mM NaCl or 50 mM NH_4Cl. [b] Error estimates for relaxation rate constants are as follows: $1/\tau_1 = \pm 5\%$; $1/\tau_2 = \pm 5\%$; $1/\tau_3 = \pm 5\%$; KIE, $\pm < 5\%$

Table 3: MVC Effects and Secondary KIEs on the Activity of the β-Reaction Resulting from Substitution of [β-^{2}H]-D,L-Ser for Isotopically Normal D,L-Ser[a,b]

Ser isotope	MVC effectors	$\nu_i/[E_0]$ (s^{-1})	isotope effect (H/D)
D,L-Ser	no MVCs	1.8	
[β-^{2}H]-D,L-Ser	no MVCs	2.2	0.8
D,L-Ser	NaCl	4.8	
[β-^{2}H]-D,L-Ser	NaCl	4.3	1.1
D,L-Ser	KCl	8.0	
[β-^{2}H]-D,L-Ser	KCl	8.7	0.9
D,L-Ser	NH_4Cl	9.6	
[β-^{2}H]-D,L-Ser	NH_4Cl	9.3	1.0

[a] Activities were measured as described under Materials and Methods. Typical conditions of concentrations are as follows: $[\alpha_2\beta_2] = 0.4\ \mu M$; [serine derivative] = 40 mM; when present, [NaCl] = 100 mM, [KCl] = 100 mM, or $[NH_4Cl]$ = 50 mM; [indole] = 0.2−0.3 mM. [b] Error limits on activity measurements were estimated to be ±10%; KIE, $\pm < 5\%$.

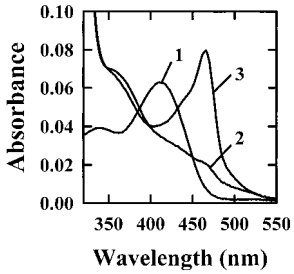

FIGURE 7: UV/vis absorbance spectra obtained after reaction of 5 μM $\alpha_2\beta_2$ with 40 mM L-Ser and indoline: enzyme alone (spectrum 1), enzyme with L-Ser and 4.5 mM indoline (spectrum 2), or enzyme with L-Ser and 4.5 mM indoline in the presence of 50 mM NH_4Cl (spectrum 3).

Ser and [β-^{2}H]-D,L-Ser are compared in the absence of MVCs, an inverse secondary KIE was found on the overall activity. The only step in the β-reaction scheme known to cause an inverse secondary KIE due to β-substitution is the formation of E(Q_3) in the reaction of E(A-A) with indole (*13*). In the presence of Na^+ or NH_4^+, no KIE was found on the turnover rate.

Primary KIEs due to the abstraction of the α-proton during formation of E(A-A) from E(Aex_1) can be detected on the turnover rate in the presence of monovalent metal ions; see the preceding paper (*1*). In the absence of monovalent metal ions and in the presence of NH_4Cl, the effect on the turnover rate is negligibly small. Table 3 summarizes the measured activities for the different isotopically substituted serines and the accompanying isotope effects. The rate of turnover in the $\alpha\beta$-reaction was not found to be subject to any kinetic isotope effects resulting from substitution of deuterium at either Cα or Cβ of serine. This finding is in agreement with rate limitation by the α-reaction under these conditions.

Ammonium Ion Effects on Activity and Distribution of Intermediates: Static UV/Visible Absorbance Analysis. Figure 7 shows the distribution of species formed at quasi-equilibrium for solutions of $\alpha_2\beta_2$, L-Ser, and indoline in the absence of MVCs (spectrum 2) and in the presence of NH_4Cl (spectrum 3). The spectrum of $\alpha_2\beta_2$ alone is also shown (spectrum 1). As is seen with the metal ions, NH_4^+ also stabilizes (albeit more weakly) the quinonoidal species.

Single-Wavelength Stopped-Flow Titration. The amplitude of the transient quinonoidal signal resulting from reaction of the E(A-A) species with indole was used to obtain an apparent dissociation constant for NH_4^+ binding. The NH_4^+ data show a slightly tighter apparent dissociation constant of 0.45 mM, versus 1.5 mM for Na^+ and 5 mM for K^+ (*14*).

Activity Measurements. Table 4 compares the relative activities of the α-, β-, and $\alpha\beta$-reactions in the presence and absence of MVCs. In agreement with the work of Woehl and Dunn (*14*), these data confirm that the rate of the α-reaction is reduced at least 3-fold by the binding of MVCs, whereas the β- and $\alpha\beta$-reactions are strongly stimulated. Under the conditions employed in Table 4, the β-reaction is stimulated 5-fold by Na^+, 6-fold by K^+, and 9-fold by NH_4^+; the $\alpha\beta$-reaction is stimulated 10-fold by Na^+, 8-fold by K^+, and 6-fold by NH_4^+. The α-reaction is inhibited 3−5-fold by Na^+, K^+, or NH_4^+.

Rapid-Scanning Stopped-Flow Measurements. RSSF measurements were performed to investigate the transient distributions of intermediates that form and decay in the pre-steady-state phase of the reaction. Figure 8 shows the reaction of $\alpha_2\beta_2$ with a mixture of L-Ser and indole in the absence (panel A) and in the presence (panel B) of NH_4Cl. As previously shown (*14*), in the absence of MVCs, the steady-state spectrum is essentially that of the E(A-A) species. In the presence of NH_4^+, however, the E(Aex_1) and E(Q_3) species dominate the spectrum. These results show that, in the absence of MVCs, the reactivity of the E(A-A) species is suppressed, whereas when NH_4Cl is present, E(A-A) readily reacts with the second substrate, just as seen with Na^+ and K^+ (*14*).

Table 4: Comparison of the Effects of MVCs on the Activities of the α-, β-, and $\alpha\beta$-Reactions Catalyzed by Tryptophan Synthase[a,b]

reaction	MVC	$v_i/[E_0]$ (s^{-1})	relative activity
α-reaction	none	0.30	1.0
	Na^+	0.09	0.3
	K^+	0.09	0.3
	NH_4^+	0.05	0.17
β-reaction	none	1.40	1.0
	Na^+	7.0	5.0
	K^+	9.0	6.0
	NH_4^+	13.0	9.0
$\alpha\beta$-reaction	none	0.32	1.0
	Na^+	3.0	10
	K^+	2.6	8.0
	NH_4^+	2.0	6.0

[a] Activities were measured under the following conditions of concentrations: [$\alpha_2\beta_2$] = 0.4 μM; [L-Ser] = 40 mM; [indole] = 0.2 mM; [IGP] = 0.2 mM; when present, [NaCl] = 100 mM, [KCl] = 100 mM, or [NH_4Cl] = 50 mM. [b] Error limits on activity measurements were estimated to be ±10%.

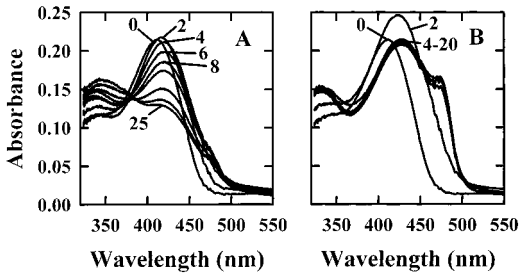

FIGURE 8: Time-resolved RSSF spectra for the reaction of $\alpha_2\beta_2$ with L-Ser and indole in the absence of MVCs (panel A) and in the presence NH_4Cl (panel B). Concentrations: [[$\alpha_2\beta_2$] = 10 μM, [L-Ser] = 40 mM, [indole] = 1 mM, and [NH_4Cl] = 50 mM where present. Timing sequence 1 was used (see Materials and Methods).

DISCUSSION

A still growing number of enzymes have been shown to be affected by MVCs (*1*, *14*, *24*−*27*). Within the past few years, significant progress has been made to determine the nature and function of those effects (*14*, *24*). The binding sites of several MVC-activated enzymes have been identified by high-resolution X-ray diffraction techniques (*16*, *17*, *28*−*31*), and the mechanisms of activation have been investigated via detailed solution studies for a few examples (*1*, *14*, *32*−*34*). These efforts have demonstrated that, in almost all cases, MVCs should be considered to be allosteric effectors acting at specific binding sites separate from the catalytic site and should transfer their effects via modulation of protein conformation to selectively influence certain binding and/or catalytic events at the active site.

Work from our laboratory (*1*, *14*) and work by Peracchi et al. (*32*) have demonstrated that the tryptophan synthase

bienzyme complex is subject to monovalent metal ion activation. Our studies showed that, in the absence of an MVC, the activity of the complex is reduced, and the allosteric cross-talk between subunits is lost. The studies presented herein and in the preceding paper (*1*) provide detailed mechanistic information about the relationship of the MVC effects, both to catalysis and to the allosteric regulation of substrate channeling in the tryptophan synthase bienzyme complex.

Metal Ion Effects on the Second Half-Reaction. The effect of MVCs on stage II (see Figures 3, 4, 7, and 9) shows characteristics somewhat different from those found for stage I; see the preceding paper (*1*). The affinity of E(A-A) for indole in the Michaelis complex is increased by metal ions about 2−3-fold. Since the rate parameters for the forward reaction of the second step are unaffected while the reverse reaction is slowed, the MVC effect is manifest as a change in amplitude for the formation of the quinonoid. The rate in the reverse direction for the second step is about 10-fold slower for the metal ion-bound state. When combined with the effect on the affinity for indole, MVC binding causes a change in the equilibrium constant in favor of quinonoid formation approaching 30-fold. As can be seen in Figure 4, the relaxation rates of formation and decay for $E(Q_3)$ are essentially unaffected by Na^+. The observed rate clearly is dominated by the rate of the forward reaction, while the amplitude of quinonoid formation dramatically increases and then saturates as the concentration of the metal ion is increased.

Mechanistic Implications of Pathway Branching. Studies of stage II using the indole analogue indoline in place of indole establish that the path of the β-reaction enters a branched segment upon formation of E(A-A) (Figure 5A). These two forms of the α-aminoacrylate species interconvert slowly and show remarkably different reactivities with indoline and, therefore, give rise to two clearly separated kinetic phases (see below). In the preceding paper (*1*), it is postulated that the less reactive species has the open conformation of the β-subunit, while the more active species has the closed conformation. The work reported herein lends further support to this hypothesis. The three-dimiensional structure of a closed conformation of the E(A-A)(5-fluoro-IGP) complex determined at 4 °C has been reported by Schneider et al. (*35*).

Indoline reacts rapidly with the activated form of E(A-A) to give $E(Q)_{indoline}$ which then turns over very slowly to form dihydroisotryptophan (*23*). Owing to the slow turnover rate, $E(Q)_{indoline}$ accumulates in a quasi-equilibrium. During the reaction of indoline with E(A-A), significantly less quinonoid is formed with the MVC-free species than with the Na^+-bound species. The titration curves in Figure 5B show that there is a pronounced difference in the apparent affinity of the enzyme for indoline in the MVC-free and Na^+-bound states, in agreement with the findings for indole (Figure 3). In the MVC-free state, the affinity is diminished at least 20-fold. However, from the measured relaxation rates (450 and 925 s^{-1} at 2 and 10 mM indoline, respectively) and the fact that the concentration dependence of the fast relaxation rate is linear in the concentration range of 0−5 mM indoline (*13*), it follows that the forward rate constant for $E(Q)_{indoline}$ formation is significantly higher for indoline than for indole. Simulation studies show that the rate is at least 10-fold higher. This increased reaction rate almost certainly reflects the considerably greater nucleophilicity of the indoline N1 in comparison to the indole C3 (*7*, *23*).

The behavior of the indoline system provides valuable insights into the reaction mechanism of the second half-reaction. The two phases for quinonoid formation associated with the Na^+-bound state are detected when E(A-A) formed in the preequilibrated mixture of enzyme and L-Ser is reacted with indoline. Simulation studies (not shown) are consistent with a mechanism wherein the fast-forming quinonoidal species results from the reaction of indoline with a preformed E(A-A) species poised to react. However, not all of the $E(Q)_{indoline}$ present at quasi-equilibrium is formed through this rapid reaction. If the slow phase were due to the readjustment of the equilibrium between the $E(Aex_1)$ and E(A-A) species (as the active form is consumed by rapid reaction with indoline), then, from the rate parameters determined for stage I, the relaxation rate expected for such a process would be about 8−9 s^{-1}. This explanation is inconsistent with the observed relaxation rate constant of 2.7 s^{-1}. The behavior of the indoline system is consistent with a mechanism in which two conformations of E(A-A) are formed from $E(Aex_1)$ (*1*). If this is true, then the relaxation rate constants and parameters observed for the first half-reaction comprise an envelope of two parallel branches. The simulations show that the indoline data are best described by a scenario in which the less active conformation of E(A-A) is formed at a rate somewhat slower than that of the active form (∼2−3 versus ∼4 s^{-1}), establishing a ratio of active to inactive conformations slightly in favor of the active conformation.

If the interconversion between the active and inactive forms of E(A-A) is slow, then the rate of interconversion must contribute to the relaxation rate constant(s) for the slow phase(s). It can be estimated that the rates for interconversion are definitely smaller than 3 s^{-1} for both the forward and the reverse reactions. The apparent affinities of both forms of E(A-A) for indoline are reduced in the absence of MVCs, and due to the change in the ratio of forms in favor of the less active species, the overall apparent affinity is considerably decreased.[2] Simulations reveal that a change in the dissociation constant of about 5-fold would result in a change

[2] While the data for reaction of the substrate analogue, indoline, with E(A-A) (see below) give valuable information on the equilibrium between the two conformations of the E(A-A) species, little insight is provided into whether the open form of the E(A-A) species is actually inactive and therefore a dead-end branch or if it is just less active than the closed conformation. The behavior of the E(A-A) species in the indole reaction shows that the pathway stays branched up to the quinonoidal species with slow rates of interconversion between conformations. It has been shown elsewhere (*1*, *14*) that the $E(Aex_1)$ species accumulates to a very high degree in the steady state. If the open E(A-A) species were completely unreactive or gave a completely unreactive, quinonoidal intermediate, then some β-sites (about 20%) would accumulate in an inactive form after the first burst of product formation. Simulation studies show that this situation would give a time trace for $E(Aex_1)$ formation demonstrating an increasing phase, corresponding in amplitude to almost 100% of the sites, followed by a decreasing phase, corresponding to accumulation of an inactive form which no longer takes part in the steady-state turnover. However, the $E(Aex_1)$ species accumulates to more than 90% of enzyme sites and shows no decreasing phase (*1*, *14*). This behavior can be simulated by postulating a mechanism with two branches, wherein one of the branches is not entirely inactive but rather is less active (see Figure 10 and Table 5).

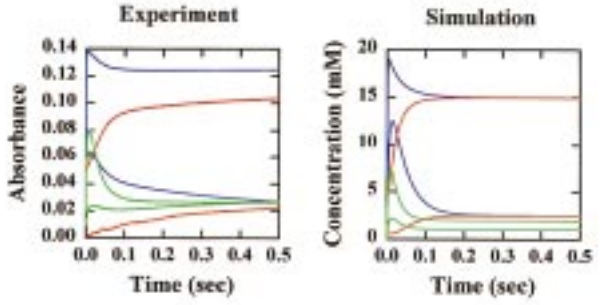

FIGURE 9: Comparisons of the simulated and experimental time courses for various steps in the β-reaction. The curves in blue show the formation and decay of the E(Aex$_1$) species in the reaction of $\alpha_2\beta_2$ with L-Ser and indole, the curves in red depict the formation of the E(Aex$_1$) species in the reaction of the E(A-A) species with indole, and the curves in green show the formation of the quinonoidal species in the reaction of the E(A-A) species with indole.

Table 5: Summary of NaCl Effects: Comparison of the Rate Parameters for Experimental and Simulated Time Courses for E(Aex$_1$) and E(Q$_{indole}$) Formation and Decay Reactions[a]

	experiment		simulation	
reaction	−NaCl	+NaCl	−NaCl	+NaCl
$\alpha_2\beta_2$ + L-Ser				
time course for E(Aex$_1$)				
$1/\tau_{formation}$	165	930	165	913
$1/\tau_{decay}$	20	8.4	20	8.8
$\alpha_2\beta_2$ + (L-Ser + indole)				
time course for E(Aex$_1$)				
$1/\tau_{formation}$	160	930	164	909
$1/\tau_{decay}$	29	32	25	30
E(A-A) + indole				
time course for E(Aex$_1$)				
$1/\tau_{formation1}$	23	27	20	40
$1/\tau_{formation2}$	2	2		
time course for E(Q$_3$)				
$1/\tau_{formation}$	190	214	166	206
$1/\tau_{decay}$	48	45	46	51

[a] Relaxation rate constants were determined from analysis of time courses following the absorbance bands of the E(Aex$_1$) species at 420 nm or of the E(Q) species at 476 nm. Simulations were carried out as described in Materials and Methods and in the text.

in the apparent affinity of about 24-fold, provided the ratio between the forms is changed from about 70% of the active form for the Na^+-bound system to about 18% for the MVC-free system (as the ratio of fast to slow phase amplitudes suggests). This change in ratio is established through the kinetics of the first half-reaction. Simulations suggest that, for the MVC-free system, the less active species of E(A-A) is formed more rapidly (up to about 18 s^{-1}), whereas the more active species is formed at about the same rate (4 s^{-1}).

Figure 9 compares the experimentally observed time courses for stage II with simulated curves constrained to the ratio of active to inactive conformations predicted by the indoline data. Table 5 compares the rate parameters used in these simulations with the experimentally determined values. Panel A of Figure 9 shows experimental time traces for the reaction of $\alpha_2\beta_2$ with a mixture of L-Ser and indole in stage II (blue time traces) and for the reaction of premixed $\alpha_2\beta_2$ and L-Ser with indole (red time traces). The formation of the quinonoidal species is also shown (green time traces). Traces are shown both for the MVC-free species and for the Na^+-bound species. Panel B shows the simulated time courses for the respective experimental curves (same coloring scheme). These curves establish a close agreement between the simulated and experimental relaxation rate parameters (see Table 5).[3]

MVC Effects on Transition States and Rate-Determining Steps. A primary KIE is detected on E(A-A) formation during stage I both in the MVC-free and in the MVC-bound species (*1*, *21*, *36*). The observed effects on the relaxation rate constants are 2.2 ± 0.2, 2.0 ± 0.2, or 3.0 ± 0.3 for the MVC-free, Na^+-bound, or NH_4^+-bound species, respectively. Detailed analyses of the kinetics for the MVC-free and Na^+-activated systems show that the intrinsic primary KIE on the specific rate constant for abstraction of the Cα proton of E(Aex$_1$) is changed from 4.0 ± 0.4 for the MVC-free state to 5.9 ± 0.5 for the Na^+-bound state (*1*), a finding consistent with the conclusion that the extent of bond scission in the transition state is altered by the binding of Na^+.

The reactions of nucleophiles with E(A-A) are accompanied by a change from an sp^2 to an sp^3 hybridization state of the L-Ser Cβ. The results with indole show that this hybridization change gives rise to an inverse secondary KIE (*13*). An inverse KIE could also be detected on the formation of E(Q$_3$) from E(A-A) and indole under all of the conditions summarized in Table 5. Consequently, these measurements establish that, in the MVC-free state, there is an inverse secondary KIE on the turnover rate resulting from the nucleophilic attack of indole on E(A-A) in stage II. In contrast to these results, when the reaction was carried out with the Na^+- or K^+-bound states, no secondary KIE could be detected on the turnover rate. The NH_4^+-bound state demonstrated neither a significant primary KIE on stage I nor a secondary KIE on the turnover rate (Table 3).

These studies show that catalysis of the β-reaction in the MVC-free system is rate limited by the nucleophilic attack of indole on the E(A-A). Hence, C−C bond formation is the dominant rate-determining process for turnover of the MVC-free system. Simulation studies for the proposed mechanism reveal that most of the enzyme sites (about 80%) accumulate as E(A-A) in the less active branch of the pathway as the reaction mixture approaches the steady state. The formation of the indole quinonoid in that branch is about 10-fold slower than in the more reactive branch. In the Na^+- or K^+-bound states, the reaction utilizes mainly the more reactive branch of the pathway. Since indole quinonoid formation via this branch is fast, formation of the E(A-A) species is rate limiting. Thus in the steady state, it is the E(Aex$_1$) species which accumulates (*14*). For this reason, a large primary KIE results from the substitution of ^2H for ^1H at the α-carbon of L-Ser. In the NH_4^+-bound state, neither

[3] The transient accumulation of the E(Aex$_1$) species is overestimated by the model. Relative amplitudes for the other species in the absence and presence of the MVC match the experimental data reasonably well. It should be kept in mind that the rate parameters used to simulate these time courses are not the result of an automated fitting procedure but represent a visual and semiquantitative test for the plausibility of the model suggested by the experimental data. The reaction pathway is too complex, and too many of the intermediates are inaccessible to direct experimental analysis to perform a complete kinetic pathway study. While the use of simulation methods is a very important tool for "proof-reading" suggested mechanisms, the simplified model assumed herein does not take into account all phases and steps in the pathway, and it is not surprising that some differences between the modeled data and experimental data arise.

C−H bond cleavage on E(Aex$_1$) nor nucleophilic addition to E(A-A) is rate determining; hence turnover must be limited by some step which follows the formation of E(Q$_2$). This conclusion is in agreement with the magnitude of the secondary isotope effects shown in Table 2. The observation of a KIE of 0.66 in the presence of NH_4^+ indicates that the interconversion of E(A-A) and E(Q$_2$) likely approaches equilibrium in this experiment.[4] In the simulation studies, the decay of E(Aex$_2$) was assumed to occur at a rate of around 20 s^{-1}. An increase in the rate of formation of the active E(A-A) species could, therefore, easily make the decay of E(Aex$_2$) rate determining. In any event, these results show that the nature of the rate-determining step for turnover is highly dependent upon interactions at the MVC site.

The NH_4^+-Activated Species. The literature on MVC binding to small molecule chelators and on MVC-activated enzymes (*24*) establishes that in almost all cases NH_4^+ is able to bind to the MVC site, giving species which mimic the properties of the corresponding K^+ complex. Indeed, NH_4^+ is considered an isosteric analogue of K^+ in most of its interactions with chelators and MVC protein sites. However, there are potentially significant differences between the coordination chemistry of NH_4^+ and the monovalent metal ions that could have important ramifications with respect to protein conformation. The group I monovalent metal ions, Li^+, Na^+, K^+, Cs^+, and Rb^+, have a single s electron outside a noble gas core, conveying spherical symmetry and low polarizability to the bonding interactions of these ions. Consequently, bonding is essentially electrostatic in nature. Coordination numbers and geometries are dependent on such factors as ligand size and charge, charge density on the metal ion, and the free energies of hydration. Both Na^+ and K^+ can form complexes containing as many as 8−10 ligands with geometries determined by the structures of the chelating molecules (see ref *24*). In contrast, NH_4^+ binding depends on H-bonding, and therefore complexes with NH_4^+ almost invariably are restricted to bonding interactions involving four acceptor atoms with a tetrahedral or distorted tetrahedral geometry. For example, the non-actin complexes of Na^+ and K^+ are eight coordinate, while the NH_4^+ complex is four coordinate (*38*). Accordingly, there is no reason, a priori, to expect that substitution of NH_4^+ for Na^+ or K^+ will give protein complexes with conformations identical to those of either the Na^+ complexes or the K^+ complexes.

Ammonium ion binds to the MVC site of tryptophan synthase with slightly higher affinity than does sodium ion or potassium ion but activates the bienzyme complex to a lesser extent than does either metal ion (see Table 4). Interestingly, NH_4^+ is a better activator for the β-reaction, stimulating the reaction 9-fold versus 5-fold for Na^+. At equilibrium, NH_4^+ stabilizes the E(Aex$_1$) species in stage I of the β-reaction to a lesser extent than does either Na^+ or K^+. However, the E(Aex$_1$) species accumulates transiently to a greater extent in the presence than in the absence of NH_4^+, just as is seen with the monovalent metal ions. In the presence of the second substrate, indole, this effect leads to a steady-state spectrum with a large contribution from the E(Aex$_1$) species. As found for the monovalent metal ions, the NH_4^+ complex gives an E(A-A) species that is more reactive toward indole. Since NH_4^+ preferentially stabilizes the more reactive form of E(A-A), it is likely that it is the tetracoordinate geometry of the MVC binding site which is important for assuming the active conformation. Crystallographic studies (*16*, *17*) indicate that this is the conformation in which βLys167 makes a salt bridge across the $\alpha-\beta$ subunit interface.

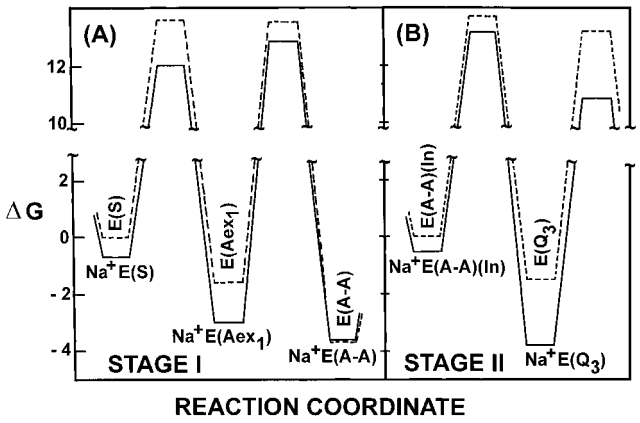

FIGURE 10: Effects of Na^+ on the free energy reaction-coordinate diagrams for stage I (A) and stage II (B) of the tryptophan synthase β-reaction. Curves: (—) Na^+-activated system and (---) MVC-free system. The free energy scale is given in kcal/mol at 25° C. Stage I ground states and activation energy barriers are shown in (A) for the interconversion of the Na^+-activated and MVC-free enzyme−substrate complexes with the corresponding E(Aex$_1$) and E(A-A) species. Stage II ground states and energy barriers are shown in (B) for the interconversion of the E(A-A)(In) Michaelis complex with E(Q$_3$) for both the Na^+-activated and MVC-free systems. In (A), the ground states of Na^+E + L-Ser, and E + L-Ser (not shown) were arbitrarily assigned the same free energy. The energy of the MVC-free E(S) complex was set at zero. In (B), the Na^+E(A-A) + indole and E(A-A) + indole ground states (not shown) were assigned the same free energy. The MVC-free E(A-A)(indole) complex was set at zero. With these conventions, the curves then compare the effects of Na^+ on the free energy diagrams. E = E(Ain), S = L-Ser, and In = indole.

Energetics of MVC Modulation of Catalysis in Tryptophan Synthase. The preceding paper (*1*) and this work present kinetic analyses that provide estimates of the specific rate constants for some of the chemical events which occur in stages I and II of the β-reaction, both for the MVC-free and for the Na^+-bound states. These data are combined into a free energy reaction-coordinate diagram (Figure 10) which compares the energy profiles for the rate-determining processes occurring in stages I and II. To facilitate these comparisons, the diagrams were constructed for two conditions: (a) the MVC-free enzyme system and (b) the Na^+-bound enzyme system. The ground states for the MVC-free and Na^+-bound E(Ain) species are arbitrarily assigned the same free energy, and the "standard state" for both systems is defined as 25 °C and pH = 7.8. For each transition state shown, the activation energy is calculated from the relationship $\Delta G^{\ddagger} = -RT(2.303)[\log k_f - \log k_r]$, where k_f is the specific rate constant for formation or decay of a species and, from transition-state kinetic theory, $k_r = (k_B T/h)K^{\ddagger}$, where k_B is the Boltzmann constant, T is absolute temperature, h is Planck's constant, and $K^{\ddagger}$ is the quasi-equilibrium constant for formation of the transition state. To construct the diagram, a value of 2.7×10^{12} s^{-1} is used for k_r. Because

[4] As pointed out by one of the reviewers, the fractionation factors of Cleland (*37*) predict an equilibrium isotope effect of approximately 0.65 for the interconversion of E(A-A) and E(Q$_2$), a value in close agreement with the observed isotope effect of 0.66 (Table 2).

$E(GD_1)$, $E(Q_1)$, and $E(Q_2)$ do not accumulate in significant amounts during stage I or II, these species are not included explicitly in the energy diagrams. The effects of MVCs on the reaction of L-Trp with E(Ain) have not been examined in kinetic detail; therefore, the portion of stage II involving $E(Aex_2)$, $E(GD_2)$, and the Michaelis complex, E(Ain)(L-Trp), has been omitted from the diagrams as well. With these omissions and simplifications, the resulting diagrams provide comparisons of the relative free energies of the ground states and transition states that dominate the kinetic and equilibrium behavior of those steps which most influence the overall kinetic behavior of the β-site.

From inspection of these data, it is clear that the binding of Na^+ has the following effects on stage I: (a) Na^+ binding slightly stabilizes the E(Ain)(L-Ser) Michaelis complex and strongly stabilizes $E(Aex_1)$ relative to the corresponding MVC-free species (*1*). (b) Na^+ binding lowers the activation energy for $E(Aex_1)$ formation while increasing the activation energy for E(A-A) formation (*1*). The effects of Na^+ on stage II are somewhat different: (a) The ground states of E(A-A)(indole) and $E(Q_3)$ are both stabilized by Na^+ binding, and this stabilization is most notable for $E(Q_3)$. (b) In contrast to stage I, the activation energies for quinonoid formation and decay are almost unaffected by Na^+ binding. (c) The pre-steady-state and steady-state data show that the α-reaction is rate determining for the $\alpha\beta$-reaction.

Functional Significance of Protein Conformational Change to Enzyme Catalysis. In the tryptophan synthase system, the dependence of intermediate distribution on the binding of allosteric effectors is a consequence of the strong influence of protein conformation on the relative ground-state stabilities and reactivities of the intermediates. While the protein no doubt exists in solution as an ensemble of conformation states, this study strongly supports the hypothesis that there exists a subset of conformational states tailored by evolution to selectively stabilize each intermediate along the reaction path (*7*, *10*, *13*−*15*, *22*, *36*, *39*−*42*). To illustrate this argument, consider the simple example involving three intermediates, X, Y, and Z. Assume that the enzyme conformation E^{ϕ} preferentially stabilizes intermediate X, while conformation E^{η} preferentially stabilizes intermediate Y and conformation E^{φ} preferentially stabilizes intermediate Z. One catalytic consequence which then follows is that selective stabilization can work to adjust the ground-state energies of the various intermediates (viz., Scheme 1) to comparable levels by providing more stabilization to species which otherwise would be high-energy intermediates than to species of inherently lower energy. According to transition-state kinetic theory, it also follows that those protein conformations that provide complementarity to the structures of the activated complexes associated with the interconversion of intermediates must decrease activation energies for those steps (*41*−*43*). In the work presented herein, the influence of MVCs and GP on the distribution of intermediates in the L-Ser reaction and in the β- and $\alpha\beta$-reactions supports the postulated existence of a subset of conformation states that are complementary to those covalent states of the PLP cofactor residing on the catalytic pathway of the β-reaction. The demonstration that selected, site-directed, single mutations at loci distant from the catalytic sites of the α- and β-subunits dramatically alter the relative stabilities of intermediates at the β-site provides further evidence of these conformation states (*20*). While not emphasized in this work, a close examination of the available UV/vis spectral data indicates that one action of the effectors (i.e., MVCs or α-site ligands) is to shift the distribution of intermediates without perturbing the electronic environment of each species (see refs *10*, *11*, *14*, *15*, *39*, and *40*). Therefore, the shifts in distribution are not accompanied by shifts in either the λ_{max} or the bandwidths of the component species (*14*, *40*). Consequently, the changes in distribution likely arise from changes in the relative stabilities of protein conformation states (e.g., the "quinonoid conformation" vs the "α-aminoacrylate Schiff base conformation"). Conversely, the altered distribution does not appear to be due to a localized alteration of the site environment which perturbs the relative stabilities of quinonoid and aminoacrylate within a single protein conformation (which should therefore also alter the microenvironment and the absorption spectrum of the chromophore). Altered reactivities then must have their origins in altered equilibria and/or altered activation energies for the conformational transitions obligatory for the chemical transformations.

On the basis of the magnitudes of the rate effects mediated by these allosteric effectors, it is evident that in the tryptophan synthase system the modulation of the catalytic pathway by allosteric interactions represents a "fine-tuning" of the catalytic properties as a consequence of evolution. The regulation of channeling also depends on the modulation of conformation at specific points in the catalytic cycle. It then is not surprising to find that the allosteric interactions which modulate catalytic events are also intertwined with the triggering of the conformational transitions between open and closed states of the $\alpha\beta$-dimeric unit. These events ensure the efficient channeling of indole between the α- and β-sites (*18*).

SUMMARY

This detailed study of MVC effects on the β- and $\alpha\beta$-reaction pathways of the tryptophan synthase bienzyme complex reveals mechanistic principles of the effector roles played by MVCs in enzyme-catalyzed reactions. The tryptophan synthase example shows that the metal ion influence cannot be assigned to a single step in the mechanism; rather, the effects are the result of specific alterations of both ground states and activation energies on several steps in the reaction pathway. These effects are manifest as a fine-tuning of the interaction between the catalytic residues in the active site and the conformational states of the enzyme.

In the second half-reaction, the MVC effect increases the affinity of E(A-A) for indole and stabilizes $E(Q_3)$. The changed ratio of open to closed E(A-A) species established in the first half-reaction is an important element in the second half-reaction as well. Under steady-state conditions, most of the MVC-free enzyme exists as a low-activity form of the E(A-A) complex, and we postulate that this species has an open conformation (*1*). If true, then the ratio of conformations favors the open, less active form of this intermediate, and the flux takes place primarily through the less active branch. Since most of the flux takes place through the more active branch in the MVC-bound forms, $E(Aex_1)$ accumulates in the steady state, and the slowest step becomes the formation of E(A-A). Consequently, the combined effects of MVC

binding on stages I and II cause a shift in the rate-determining step of the β-reaction.

Another aspect of the change in ratio of open to closed forms derives from the importance of these conformational changes to the allosteric interaction between subunits. The formation of a closed conformation in the β-subunit helps to stabilize the closed conformation of the α-subunit−IGP complex and stimulates the rate of the β-reaction (*14*, *15*, *44*). The analysis of the ammonium ion effect suggests that the conformation state of the putative tetracoordinate metal ion binding site, the conformation identified by Rhee et al. (*16*, *17*) with the βK167−αD56 salt bridge across the $\alpha\beta$-subunit interface, is the conformation responsible for shifting the equilibrium toward the more reactive E(A-A) species. Further analysis using tryptophan synthase derivatives with mutations in residues important to the conformational transition from open to closed has provided additional insight into the mechanistic details of the role played by the metal ions in transmitting allosteric signals across the subunit interface (*20*).

REFERENCES

1. Woehl, E., and Dunn, M. F. (1999) *Biochemistry, 38*, 7118−7130.
2. Yanofsky, C., and Crawford, I. P. (1972) in *The Enzymes, 3rd Ed.* (Boyer, P. D., Ed.) pp 1−31, Academic Press, New York.
3. Miles, E. W. (1979) *Adv. Enzymol. Relat. Areas Mol. Biol. 49*, 127−186.
4. Miles, E. W. (1991) *Adv. Enzymol. Relat. Areas Mol. Biol. 64*, 93−172.
5. Miles, E. W. (1991) *J. Biol. Chem. 266*, 10715−10718.
6. Hyde, C. C., Ahmed, S. A., Padlan, E. A., Miles, E. W., and Davies, D. R. (1988) *J. Biol. Chem. 263*, 17857−17871.
7. Dunn, M. F., Aguilar, V., Brzovic, P. S., Drewe, W. F., Jr., Houben, D. F., Leja, C. A., and Roy, M. (1990) *Biochemistry 29*, 8598−8607.
8. Lane, A. N., and Kirschner, K. (1991) *Biochemistry 30*, 479−484.
9. Anderson, K. S., Miles, E. W., and Johnson, K. A. (1991) *J. Biol. Chem. 266*, 8020−8033.
10. Brzovic, P. S., Ngo, K., and Dunn, M. F. (1992) *Biochemistry 31*, 3831−3839.
11. Brzovic, P. S., Sawa, Y., Hyde, C. C., Miles, E. W., and Dunn, M. F. (1992) *J. Biol. Chem. 267*, 13028−13038.
12. Brzovic, P. S., Hyde, C. C., Miles, E. W., and Dunn, M. F. (1993) *Biochemistry 32*, 10404−10413.
13. Leja, C. A., Woehl, E. U., and Dunn, M. F. (1995) *Biochemistry 34*, 6552−6561.
14. Woehl, E. U., and Dunn, M. F. (1995) *Biochemistry 34*, 9466−9476.
15. Pan, P., and Dunn, M. F. (1996) *Biochemistry 35*, 5002−5015.
16. Rhee, S., Parris, K. D., Ahmed, S. A., Miles, E. W., and Davies, D. R. (1996) *Biochemistry 35*, 4211−4221.
17. Rhee, S., Parris, K. D., Hyde, C. C., Ahmed, S. A., Miles, E. W., and Davies, D. R. (1997) *Biochemistry 36*, 7664−7680.
18. Pan, P., Woehl, E., and Dunn, M. F.(1997) *Trends Biochem. Sci. 22*, 22−27.
19. Miles, E. W., Rhee, S., and Davies, D. R. (1999) *J. Biol. Chem. 274*, 12193−12196.
20. Woehl, E. U., Banik, U., Hur, O., Farrari, D., Bagwell, C., Miles, E. W., and Dunn, M. F. (1999) *Biochemistry* (in preparation).
21. Lane, A. N., and Kirschner, K. (1983) *Eur. J. Biochem. 129*, 561−570.
22. Drewe, W. F., Jr., and Dunn, M. F. (1986) *Biochemistry 25*, 2494−2501.
23. Roy, M., Keblawi, S., and Dunn, M. F. (1988) *Biochemistry 27*, 6698−6704.
24. Woehl, E. U., and Dunn, M. F. (1995) *Coord. Chem. Rev. 144*, 147−197.
25. Suelter, C. H. (1970) *Science 168*, 789−795.
26. Suelter, C. H. (1974) in *Metal Ions in Biological Systems*, Marcel Dekker, New York.
27. Evans, H. J., and Sorger, G. J. (1966) *Annu. Rev. Plant Physiol. 17*, 47−76.
28. Toney, M. D., Hohenester, E., Keller, J. W., and Jansonius, J. N. (1995) *J. Mol. Biol. 245*, 151−179.
29. Antson, A. A., Demidkia, T. V., Gollnick, P., Dauter, Z., Von Tersch, R. L., Long, J., Berezhnoy, S. N., Phillips, R. S., Harutyunyan, E. H., and Wilson, K. S. (1993) *Biochemistry 32*, 4195−4206.
30. Isupov, M. N., Antson, A. A., Dodson, G. G., Dementieva, I. S., Zakomirdina, L. N., and Harytyunyan, E. H. (1994) in *Biochemistry of Vitamin B6 and PQQ* (Marino, G., Sanna, G., and Bossa, F., Eds.) (in press).
31. Larson, T. M., Laughlin, L. T., Holden, H. M., Rayment, I., and Reed, G. H. (1994) *Biochemistry 33*, 6301−6309.
32. Peracchi, A., Mozzarelli, A., and Rossi, G. L. (1995) *Biochemistry 34*, 9459−9465.
33. Wells, C. M., and Di Cera, E. (1992) *Biochemistry 31*, 11721−11730.
34. Chen, H., and Phillips, R. S. (1993) *Biochemistry 32*, 11591−11599.
35. Schneider, T. R., Gerhardt, E., Lee, M., Liang, P.-H., Anderson, K. S., and Schlichting, I. (1998) *Biochemistry 37*, 5394−5406.
36. Drewe, W. F., Jr., and Dunn, M. F. (1985) *Biochemistry 24*, 3977−3987.
37. Cleland, W. W. (1980) *Methods Enzymol. 64*, 104−125.
38. Dobler, M. (1981) *Ionophores and Their Structures*, pp 5, 39, Wiley, New York.
39. Houben, K. F., and Dunn, M. F. (1990) *Biochemistry 29*, 2421−2429.
40. Houben, K. F., Kadima, W., Roy, M., and Dunn, M. F. (1989) *Biochemistry 28*, 4140−4147.
41. Pauling, L. (1948) *Am. Sci. 36*, 51.
42. Bernhard, S. A. (1983) The coupling of conformation change to covalent bond change in enzyme catalysis, *Oholo Symposium on Transition States and Enzyme Reaction Mechanisms* (Chipman, D., and Green, B., Eds.) Elsevier, Amsterdam.
43. Wolfenden, R. (1969) *Nature 223*, 704.
44. Brzovic, P. S., Miles, E. W., and Dunn, M. F. (1991) in *Proceedings of the 8th International Congress on Vitamin B6 and Carbonyl Catalysis* (Wada, H., Soda, K., Fukui, T., and Kagamiyama, H., Eds.) pp 277−280, Pergamon Press, New York.

BI982919P